A Single Amino Acid Replacement Results in the Ca^{2+}-Induced Self-Assembly of a Helical Conantokin-Based Peptide†

Qiuyun Dai, Francis J. Castellino, and Mary Prorok*

Department of Chemistry and Biochemistry and the W. M. Keck Center for Transgene Research, University of Notre Dame, Notre Dame, Indiana 46556

Received June 9, 2004; Revised Manuscript Received August 2, 2004

ABSTRACT: Conantokins are short (17−27 amino acid residues), γ-carboxyglutamate (Gla)-rich peptide components of the venoms of marine snails of the genus *Conus*. They display high apo and/or Ca^{2+}-induced helicity and act as potent and selective inhibitors of the *N*-methyl-D-aspartate receptor (NMDAR). We have previously established that one of the conantokins, conantokin-G (con-G), self-associates in the presence of Ca^{2+} with high specificity for antiparallel chain orientation [Dai, Q., Prorok, M., and Castellino, F. J. (2004) *J. Mol. Biol. 336*, 731−744]. The dimerization appears to be driven by interhelical Ca^{2+} coordination between the following residue pairings: Gla^3-$Gla^{14'}$, Gla^7-$Gla^{10'}$, Gla^{10}-$Gla^{7'}$, and Gla^{14}-$Gla^{3'}$. A second member of the conantokin family, conantokin-T (con-T), shares sequence identity with con-G at 8 of 21 amino acids, including 4 Gla residues. These similarities notwithstanding, several primary and secondary structural differences exist between con-T and con-G. Particularly notable is that con-T contains a Lys, rather than a Gla, at position 7. Moreover, unlike con-G, con-T does not undergo Ca^{2+}-triggered self-assembly. In the present study, sedimentation equilibrium ultracentrifugation is employed to demonstrate that a single amino acid replacement analogue of con-T, con-T[K7γ], assumes a dimeric superstructure in the presence of Ca^{2+} at pH values consistent with the ionization of Gla carboxylate groups. Furthermore, HPLC-monitored thiol−disulfide folding and rearrangement assays with Cys-containing con-T variants suggest that the relative chain alignment preference in the noncovalent complex is antiparallel. Our results suggest that interchain Ca^{2+} coordination in con-T[K7γ] is incumbent upon an "*i*, *i* + 4, *i* +7, *i* +11" arrangement of Gla residues, as occurs in native con-G.

Helix−helix interactions, such as those that occur in coiled-coil domains (*1*−*3*), four-helix bundles (*4*), membrane-spanning helical bundles (*5*), or EF hands (*6*), are important to the structural organization and function of numerous proteins. In engineered proteins or peptides, a firm understanding of the noncovalent forces that influence such folding patterns is necessary for the successful incorporation and manipulation of desired superstructural motifs. In several natural proteins and model peptide systems, metal ions can aid in the formation of coiled coils and helical bundles through stabilization of preexisting folded components into superstructures (*7*−*9*) or by directing the folding and subsequent assembly of polypeptide chains (*10*−*13*). In both categories, while cooperative metal ion coordination among subunits initiates oligomerization and/or guides relative chain orientation, hydrophobic interactions at the interchain interface remain the predominant forces that drive and stabilize complex formation.

Recently, we have found that synthetic conantokin-G (con-G),[1] a 17-residue, γ-carboxyglutamate (Gla, γ)-rich neuroactive peptide (GEγγLQγNQγLIRγKSN-NH_2) derived from the venom of *Conus geographus*, self-associates in the presence of Ca^{2+} to form a helical dimer with an antiparallel orientation (*14*). To our knowledge, con-G is the smallest naturally occurring peptide to undergo metal ion mediated self-assembly. This superstructure is also unusual in the realm of helix−helix interactions because the bulk of the binding energy associated with subunit association appears to derive from interhelical Gla−Ca^{2+} coordination, rather than hydrophobic interactions. On the basis of sedimentation equilibrium results obtained with individual Gla replacement analogues of con-G, we have identified the following Gla residues as interhelical Ca^{2+} coordination partners: Gla^3−$Gla^{14'}$, Gla^7−$Gla^{10'}$, Gla^{10}−$Gla^{7'}$, and Gla^{14}−$Gla^{3'}$. A second member of the conantokin family, conantokin-T (con-T; GEγγYQKMLγNLRγAEVKKNA-NH_2) from *Conus tulipa* (*15*), shares sequence identity with con-G at eight sequence positions, including the four positions occupied by Gla residues. Aside from these similarities, conspicuous primary sequence differences exist between the two peptides, namely, length (con-T is four residues longer than con-G) and the distinct lack of conservation among the nonidentical residues (only position 12 is conserved). Regarding the latter set of

† This work was supported by National Institutes of Health Grant HL-19982 to F.J.C.

* Corresponding author: Mary Prorok, Department of Chemistry & Biochemistry, 251 Nieuwland Hall, University of Notre Dame, Notre Dame, IN 46556. Tel: (574) 631-9120. Fax: (574) 631-4048. E-mail: mprorok@nd.edu.

[1] Abbreviations: CD, circular dichroism; con-G, conantokin-G; con-T, conantokin-T; ITC, isothermal titration calorimetry; Gla, γ-carboxyglutamic acid; Mes, 4-morpholineethanesulfonic acid; NMDAR, *N*-methyl-D-aspartate receptor; TFA, trifluoroacetic acid.

10.1021/bi048796s CCC: $27.50
Published on Web 09/25/2004

differences, the most striking resides with sequence position 7, which is Gla in con-G and Lys in con-T. The two peptides also have pronounced secondary structural characteristics: Con-G exhibits minimal structure in its metal-free form, yet assumes pronounced, end-to-end helicity in the presence of divalent metal cations (*16*−*20*). In contrast, con-T is highly helical in the absence of metal ions as well as in metal ion loaded form (*16*, *17*, *21*). Con-T also displays greater affinity for Ca^{2+} and Mg^{2+} compared with con-G (*16*, *22*). These differing properties can, in part, be ascribed to the nature of the residue occupying sequence position 7. For apo-con-G, the presence of Gla^7 introduces a continuum of of i, $i + 3$, and i, $i + 4$ electrostatic repulsions, obviating helix formation whereas, in the case of con-T, a Lys at position 7 facilitates helix-stabilizing side-chain interactions, viz., those between Gla^3 and Lys^7, Gla^4 and Lys^7, and Lys^7 and Gla^{10} (*17*, *21*). Pertinent to the present study, another salient difference between the two peptides includes the observation that con-T, unlike con-G, does not self-associate in the presence of Ca^{2+} (*14*). This incongruity is addressed herein by examining the relationship of Gla arrangement, with emphasis on sequence position 7, to the associative tendencies of con-T-based peptides.

MATERIALS AND METHODS

Peptide Synthesis, Purification, and Characterization. The methods for synthesis, purification, and characterization of non-Cys- and reduced Cys-containing peptides, as well as the oxidative formation of the disulfide-linked homostranded peptides (di-C^0-con-T[K7γ] and di-con-T[K7γ,V17C]) and the heterostranded species, C^0-con-T[K7γ]/con-T[K7γ,V17C], were similar to those previously described (*14*).

Determination of Peptide Strand Orientation. Strand orientation preference was determined using con-T[K7γ,V17C] and C^0-con-T[K7γ]. Typically, a 1:1 molar ratio of con-T[K7γ,V17C] and C^0-con-T[K7γ] at concentrations of 0.3−0.5 mM were stirred in an open vial at room temperature in a total volume of 0.5 mL of folding buffer (50 mM $NaBO_3$/100 mM NaCl, pH 8.2). The progress of the oxidation was monitored by analytical reverse-phase HPLC as follows: Volumes of 20 μL were injected onto an HPLC equipped with a Vydac C_{18} column (218TP, 4.6 mm × 250 mm) equilibrated in 95% of 0.1% TFA and 5% of 0.1% TFA/CH_3CN at a flow rate of 1.0 mL/min. At a time of 2 min postinjection, a 40 min gradient of 10−35% 0.1% TFA/CH_3-CN was implemented to elute the peptides. The absorbency was monitored at 214 nm. Product peaks were individually collected and identified by DE-MALDI-TOF spectrometry.

The thiol−disulfide rearrangement experiments were carried out under conditions similar to the above folding procedure. The homostranded disulfide-linked peptides (di-C^0-con-T[K7γ] or di-con-T[K7γ/V17C]) were dissolved in folding buffer at a concentration of 220 μM. An aliquot of reduced con-T[K7γ,V17C] was added to the di-C^0-con-T[K7γ] solution. Conversely, an aliquot of reduced C^0-con-T[K7γ] was introduced into the di-con-T[K7γ,V17C]. In either case, the initial disulfide/reduced monomer molar ratio was 1:2. $CaCl_2$ or $MgCl_2$ was immediately added for a final concentration of 20 mM or 10 mM, respectively. Aliquots were removed at selected intervals and analyzed by analytical reverse-phase HPLC as described for the oxidation of the reduced peptides.

Circular Dichroism. CD spectra were recorded between 195 and 260 nm on an AVIV Model 202SF spectrometer as detailed earlier (*14*).

Isothermal Titration Calorimetry (ITC). The binding isotherms of metal ions to con-T and con-T[K7γ] were determined at 25 °C on a VP-ITC microcalorimeter (MicroCal, Inc., Northampton, MA) using procedures similar to those described previously (*14*). Peptides were dissolved in 10 mM Na-Mes, 100 mM NaCl, pH 6.5, for a final concentration in the reaction cell of 0.3−0.5 mM. Titrant solution consisting of $CaCl_2$ or $MgCl_2$ (ca. 15 mM), in matching Mes buffer, was delivered at 200 s intervals. For each experiment, the heats of $CaCl_2$ or $MgCl_2$ dilution were determined in the absence of peptide and subtracted from the total heat changes observed. Corrected titration curves were deconvoluted for the best fit model using the ORIGIN for ITC software package supplied by MicroCal.

Analytical Ultracentrifugation. Sedimentation equilibrium experiments were performed with on a Beckman Optima XL-I analytical ultracentrifuge (Palo Alto, CA) equipped with an An-60 Ti rotor. All peptides were dissolved in 10 mM sodium borate/100 mM NaCl buffer at pH 6.5 or pH 8.0 (with the exception of the pH-dependence experiment) at a concentration of 150 μM, and introduced into standard two-channel cells. The peptide samples in the absence and presence of the indicated divalent metal ion (chloride salt) were independently rotated at 32000 and 45000 or 52000 rpm at 20 °C for 25 h. Absorbance monitoring was performed at 275 nm. The apparent molecular weight (MW_{app}) was obtained by fitting the data to a single ideal species or self-association using the sedimentation analysis software supplied by Beckman. The partial specific volumes used were 0.719 mL/g and 0.711 mL/g for con-T and con-T[K7γ], respectively, and were calculated from the mass average of the partial specific volumes of the individual amino acids. The partial specific volume of Gla was assigned that of Glu.

RESULTS

Replacement of Lys^7 with Gla Results in Ca^{2+}-Induced Self-Assembly of Con-T. The primary sequences of con-T and related peptides relevant to this study, as well as their α-helical heptad repeat assignments (a−g or a′−g′), are shown in Figure 1. Sedimentation equilibrium, CD, and ITC data for con-T and con-T[K7γ] in the presence or absence of Ca^{2+} and Mg^{2+} are listed in Table 1. Both peptides bind Ca^{2+} and Mg^{2+} and undergo substantial increases in helicity as a consequence, although the absolute value of the CD-derived helical content of metal-free con-T[K7γ] is considerably less than that of con-T (12% versus 55%), consonant with the negligible helicity associated with apo-con-G (*16*, *20*). Oligomerization of con-T was not noted in either apo or metal ion complexed forms. Upon replacement of Lys^7 with Gla, the resulting analogue also displayed monomeric behavior under metal ion free conditions. However, the apparent molecular weight (MW_{app}) of con-T[K7γ] (150 μM) was effectively doubled from 3390 to 6660 upon addition of 20 mM Ca^{2+} (Figure 2).[2] Essentially identical MW_{app} values were obtained for the apo- and Ca^{2+}-loaded forms of con-T[K7γ] at peptide concentrations of 300 μM, strongly suggesting that the dimeric complex is the largest higher order species attainable under the cited conditions (data not

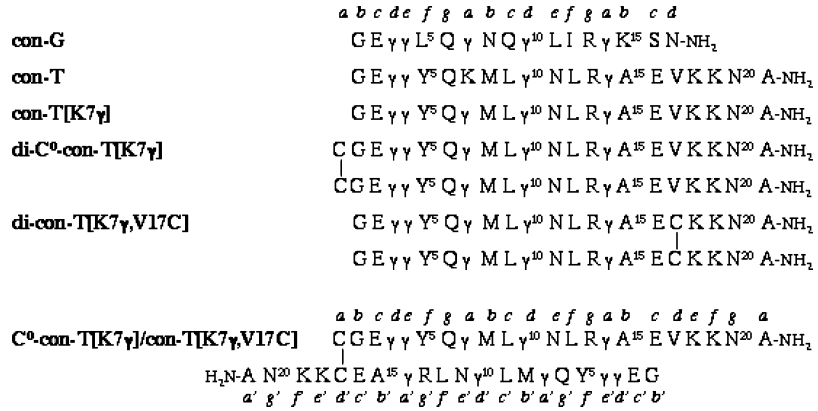

FIGURE 1: Primary sequences of the conantokin peptides used in the study. The positions of individual amino acids in the helical heptad repeat are denoted $a-g$ and $a'-g'$ (for antiparallel strands).

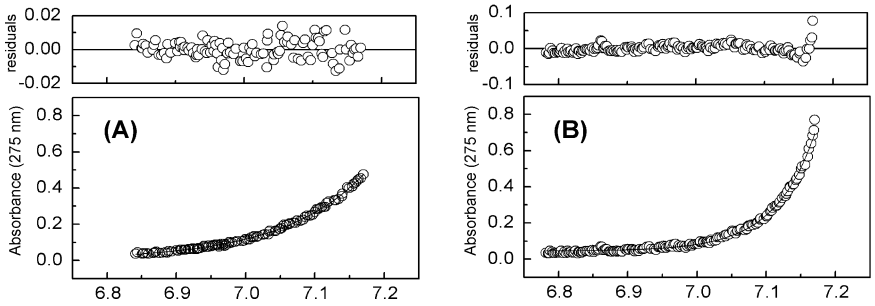

FIGURE 2: Sedimentation equilibrium scans (bottom panels) for con-T[K7γ] (150 μM) in 10 mM $NaBO_3$, 100 mM NaCl (pH 6.5) in the (A) absence and (B) presence of $CaCl_2$ (20 mM). The data were collected at rotor speeds of 52000 rpm. The fitted MW_{app} values corresponding to these data were 3300 for A and 6700 for B. The distributions of residuals for the calculated fits are displayed in the top panels. Similar values for MW_{app} were obtained from experiments conducted at rotor speeds of 45000 rpm.

shown). The low stoichiometry of Ca^{2+} binding to con-T[K7γ], ca. 3 mol of Ca^{2+}/mol of peptide, discounts the possibility that the increase in MW_{app} is attributable to complexed Ca^{2+}. As previously found for con-G (*14*), other alkaline-earth metal ions, including Ba^{2+} and Sr^{2+}, also induce the self-assembly of con-T[K7γ]. However, neither Mg^{2+}, Zn^{2+}, nor Mn^{2+} facilitates association, despite the higher content of α-helix in these metal ion/peptide complexes compared to Ca^{2+}-bound con-T[K7γ] (Table 1). The MW_{app} values of the Gla-deficient con-T analogues, con-T[K7γ,γ3A], con-T[γ10A], and con-T[γ14A], were also determined in the absence and presence of Ca^{2+}. In all cases, only monomeric MW_{app} values were noted for these peptides (data not listed).

The dependence of the MW_{app} of con-T[K7γ] on Ca^{2+} concentration is clearly shown in Figure 3A. The EC_{50} associated with the Ca^{2+}-assisted transition is 0.45 mM. The MW_{app} at the plateau (6750) corresponds to the dimeric value. The ability of Mg^{2+} to displace Ca^{2+} as an intra- but not an intermolecular ligand is also presented in Figure 2A. The EC_{50} of Mg^{2+} for reversal of the Ca^{2+}-mediated dimerization is 0.28 mM. Thus, while Mg^{2+} binds con-T[K7γ] more tightly than Ca^{2+}, it cannot support interchain association.

The self-association of con-T[K7γ] in the presence of Ca^{2+} also exhibits pH dependence. As shown in Figure 3B, con-T[K7γ] displays a monomeric MW_{app} at pH 3.5, despite the

Table 1: Metal Ion Effects on the Secondary Structure and Self-Associative Properties of Con-T and Con-T[K7γ]

peptide	metal ion[a]	% helix[b]	MW_{app}[c]	n[d]	K_d[d] (μM)
con-T	none	55	3160		
	Ca^{2+}	72	3240	0.8[e]	428[e]
	Mg^{2+}	82	3290	0.8[e]	10[e]
con-T[K7γ]	none	12	3390		
	Ca^{2+}	67	6660	2.8	120
	Mg^{2+}	74	3330	1.6	18
	Zn^{2+}	72	3750		
	Mn^{2+}	70	3700		
	Ba^{2+}	50	10080		
	Sr^{2+}	52	7060		

[a] For both CD and analytical ultracentrifugation experiments, the metal ion concentrations employed were 20 mM for Ca^{2+}, Mg^{2+}, Ba^{2+}, and Sr^{2+} and 5 mM for Zn^{2+} and Mn^{2+}. In all cases, the chloride salts were used. [b] Percentage of helix was determined from CD measurements as described earlier (*16*). [c] Values for MW_{app} were derived from 2 to 4 separate sedimentation equilibrium analyses. In all cases the error estimate for replicate experiments was ≤8%. [d] Values for n (stoichiometry of metal ion binding) and K_d were determined by ITC as indicated in Materials and Methods. [e] Excerpted from a previously published study (*22*).

[2] The calculated sequence-based apo monomeric MW for con-T[K7γ] = 2724. While the MW_{app} determined from sedimentation equilibrium of metal-free, presumably monomeric, con-T[K7γ] is higher than the calculated value, the random distribution of residuals attending the fit to a single ideal species, as shown in Figure 2A, is a reliable indicator of monomeric solution behavior. The disparity in calculated versus experimental MW may, in part, reside with the artificially high partial specific volume of 0.711 mL/g assigned to the con-T[K7γ]. Because the partial specific volume of Gla has not been reported, we assigned to it the Glu value of 0.66 mL/g. This is almost certainly an overestimate when considering that the additional carboxylate in the Gla side chain should effectively lower the partial specific volume relative to Glu. When the high percentage of Gla in con-T[K7γ] is considered, the effect of incorporating an incorrect partial specific volume for Gla can lead to a significant overestimate of MW_{app}. The same rationale can also be extended to the discrepancy in the experimentally determined versus sequence-based MW for con-T. These discrepancies notwithstanding, we emphasize that the relative MW_{app} values strongly argue for a monomer−dimer equilibrium.

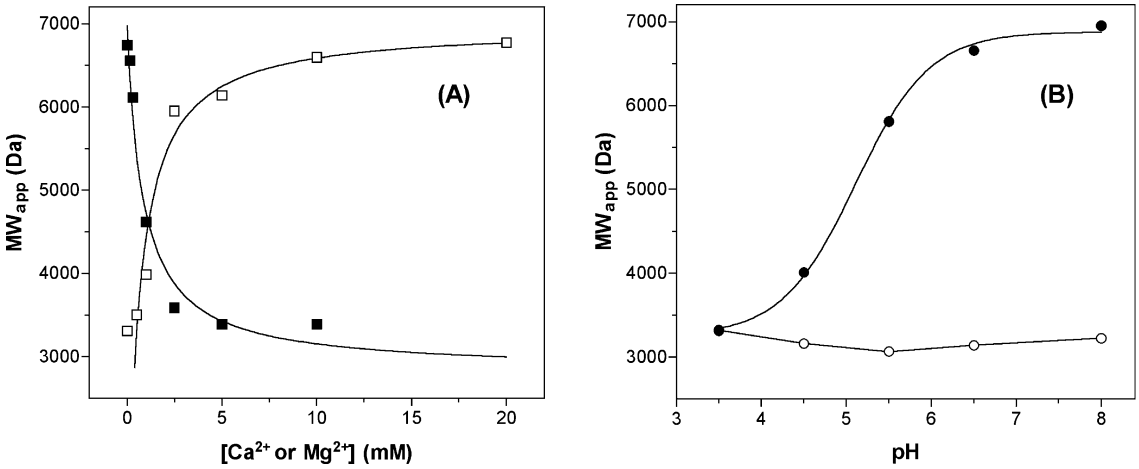

FIGURE 3: Effects of divalent ion concentration and pH on the MW_{app} of con-T[K7γ] as determined by sedimentation equilibrium. Peptide concentration in all cases was 150 μM. (A) The effect of $CaCl_2$ (□) on the self-association of con-T[K7γ] in 10 mM $NaBO_3$, 100 mM NaCl, pH 6.5; the effect of $MgCl_2$ (■) on the monomer−dimer equilibrium of con-T[K7γ] in 10 mM $NaBO_3$, 100 mM NaCl, 20 mM $CaCl_2$, pH 6.5. Fits (solid lines) were obtained from nonlinear regression analysis of the data described by the simple hyperbolic equation for one-site binding, $MW_{app} = (MW_{app(max)} \times M^{2+})/(EC_{50} + M^{2+})$, where M^{2+} is either Ca^{2+} or Mg^{2+} and EC_{50} is the metal ion concentration at which half of the sites involved in dimerization are occupied. (B) The influence of pH on con-T[K7γ] oligomerization in the (○) absence and (●) presence of Ca^{2+} (20 mm). Peptide was dissolved in 100 mM NaCl. The pH was adjusted by the addition of 1 N NaOH or HCl. The data for the Ca^{2+}-containing titration were fitted to the logistic equation: $MW_{app} = MW_{app(initial)} + (MW_{app(max)} - MW_{app(initial)})/(1 + 10^{pHmid-pH})$, where pH_{mid} is the midpoint of the transition from monomeric ($MW_{app(initial)}$) to dimeric ($MW_{app(max)}$) molecular weight.

presence of 20 mM Ca^{2+}. With each incremental pH increase, an increasing amount of con-T[K7γ] association occurs, suggesting that the formation of the higher order species relies on the ionization of one or more acidic side chains, which include Glu^2, Glu^{16}, and Gla residues 3, 4, 7, 10, 14. A fit of the limited data for the pH-induced dimerization provided a pH midpoint of 5.1. The ratio of molar ellipticities at 222 and 208 nm ($[\Theta_{222}]/[\Theta_{208}]$) is also Ca^{2+}- and pH-dependent (Figure 4). At Ca^{2+} concentrations of 5 mM and higher, and at pH values of 5 and above, the $[\Theta_{222}]/[\Theta_{208}]$ ratio is greater than 1. Though not an uncontestable indicator of supercoiling (*23*), a $[\Theta_{222}]/[\Theta_{208}]$ ratio of greater than 1 is generally regarded as diagnostic of coiled-coil structure, and perhaps other interacting helices (*24*, *25*). The inflection points for the CD-monitored Ca^{2+} and pH titrations correspond to 0.70 mM and 4.40 pH units, respectively. These values, similar to those extracted from the data in Figure 3, imply that an increase in peptide helicity is coincident with the self-association event.

When examined at different Ca^{2+} concentrations, the CD-monitored temperature dependence of the band intensities of con-T[K7γ] at 208 and 222 nm is markedly different (Figure 5A). At low Ca^{2+} levels (0.2 mM), where the monomeric form of the peptide prevails, the intensities of the minima at 208 and 222 nm decrease in a nearly parallel manner with increasing temperature. However, for the melting curve conducted at high Ca^{2+} concentration (20 mM), a steeper temperature-dependent decrease in band intensity at 222 nm versus 208 nm is observed. This is consistent with the presence of interacting helices for which the change at 222 nm reflects strand dissociation as well as monomeric helix unfolding, whereas the ellipticity at 208 nm only reports monomer unfolding. An examination of the effect of guanidine-HCl on peptide denaturation at different con-T[K7γ] concentrations also reinforces the existence of reversible peptide oligomerization under saturating Ca^{2+} conditions (Figure 5B). As is consistent with a concentration-imposed shift in the monomer−dimer equilibrium, the higher concentration of peptide (150 μM) is clearly more refractory to unfolding than the more dilute (30 μM) sample.

Helical Strand Orientation in Con-T[K7γ]/Ca^{2+}. In order to determine the relative strand alignment, i.e., parallel or antiparallel, of the Ca^{2+}-loaded con-T[K7γ] dimer, we designed two Cys-containing con-T[K7γ] variants as follows: con-T[K7γ,V17C] which contains a Cys substitution at the C-terminal Val^{17}, and C^0-con-T[K7γ], in which a Cys residue precedes the N-terminal Gly. Because our initial model of the con-T[K7γ] helical dimer consisted of a Gla core (designated as positions *a* and *d* in the heptad template) involving Gla residues 3, 7, 10, and 14, the placement of Cys in each variant also occurs at position *a* or *d* in the heptad repeat (Figure 1). Using the two Cys-containing variants, the preference for relative helix orientation was assessed by examining relative amounts of oxidized product (*26*−*28*). The distribution of products resulting from co-incubation of C^0-con-T[K7γ] and con-T[K7γ,V17C] in the absence and presence of various metal ions is shown in the series of chromatograms in Figure 6. With Ca^{2+} present, the main oxidative product is the "antiparallel" heterodimer (C^0-con-T[K7γ]/con-T[K7γ,V17C]) which predominates over the homostranded products, di-C^0-con-T[K7γ] and di-con-T[K7γ,V17C], at a ratio of 17:4:1. Among the other metal ions tested, Sr^{2+} partly mimics the action of Ca^{2+} while Mg^{2+}, Ba^{2+}, and Mn^{2+} are far less effective at directing the formation of a specific disulfide-bonded species. In the presence of Mg^{2+}, for example, the ratio of heterodimer, di-C^0-con-T[K7γ], and di-con-T[K7γ,V17C] is ca. 3:3:1. In the absence of any metal ion or in the presence of metal ions other than Ca^{2+}, the final oxidation product distribution was attained after ca. 4 h, while heterodimer formation in the presence of Ca^{2+} was completed in less than 30 min. These time course results indicate that, in Ca^{2+}-containing folding buffer, the "antiparallel" heterostranded species is both kinetically and thermodynamically favored.

The preference of antiparallel helix orientation is further supported by the results of related thiol−disulfide exchange

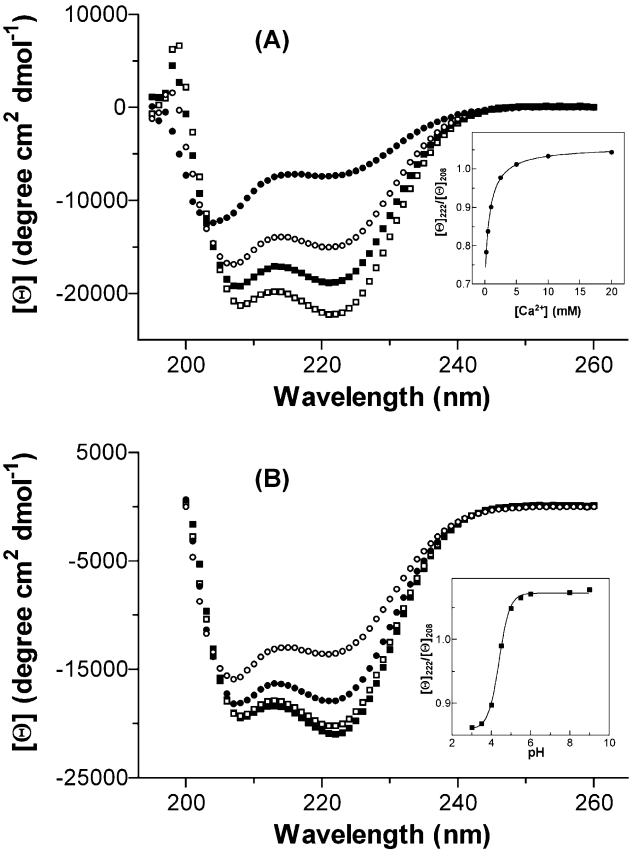

FIGURE 4: CD-monitored Ca^{2+} and pH titrations of con-T[K7γ]. (A) Representative wavelength scans from the titration of 150 μM con-T[K7γ] with $CaCl_2$ in 10 mM $NaBO_3$, 100 mM NaCl, pH 6.5: (●) 0 mM Ca^{2+}; (○) 1 mM Ca^{2+}; (■) 2.5 mM Ca^{2+}; (□) 20 mM Ca^{2+}. Inset: The ratio of molar ellipticities at 222 and 208 nm as a function of added Ca^{2+} for the full complement of points employed in the titration. An EC_{50} for Ca^{2+} of 0.71 mM was obtained from a nonlinear regression analysis of the data described by the simple hyperbolic equation for one-site binding, as described in the caption to Figure 3. (B) Representative wavelength scans from the pH titration of 150 μM con-T[K7γ]. Peptide was dissolved in 100 mM NaCl, 20 mM $CaCl_2$ and adjusted for the desired pH using 1 N HCl or NaOH: (○) pH 3.0; (●) pH 4.5; (□) pH 5.0; (■) pH 9.0. Inset: The ratio of molar ellipticities at 222 and 208 nm as a function of pH for the full complement of pH values used in the titration. Data were fit to the logistic equation, as described in the caption to Figure 3.

experiments (*29*, *30*) in which the homodimeric disulfides were individually incubated with C^0-con-T[K7γ] and con-T[K7γ,V17C] (Figure 7). Beginning with con-T[K7γ,V17C] and di-C^0-con-T[K7γ] in a 2:1 molar ratio in the presence of Ca^{2+}, the heterodimeric product is the prevalent species at equilibrium. However, with Mg^{2+} present in this folding buffer, formation of the heterostrand is minimal. The heterodimer also formed, albeit not completely, in the complement experiment in which C^0-con-T[K7γ] and di-con-T[K7γ,V17C] were the initial reactants. These data indicate that the homostranded peptides are not the most stable disulfide products, and will exchange with reduced peptide to form the heterostranded species. In addition, in the presence of Ca^{2+}, the heterodimer is completely resistant to scrambling upon the introduction of C^0-con-T[K7γ] or con-T[K7γ,V17C] (data not shown), further underscoring the Ca^{2+}-linked stability of this species. These results conclusively demonstrate that, in Ca^{2+}-containing buffer, the heterodimeric peptide is more stable than either homodimer. Extrapolating to the reversibly associating system, we conclude that the Ca^{2+}-triggered self-assembly of con-T[K7γ] into a dimeric superstructure occurs with antiparallel strand orientation.

DISCUSSION

We have previously found that the Ca^{2+}-assisted self-association of the naturally occurring conantokin peptide, con-G, appears contingent upon an "*i*, *i* + 4, *i* +7, *i* + 11" arrangement of Gla residues (*14*). Broadly speaking, the con-G/Ca^{2+} complex is a dimeric assembly of highly helical strands, but the driving force directing the self-organization is distinguished from canonical coiled coils and helical bundles insofar as it appears to originate and be maintained by electrostatics rather than hydrophobic effects. Con-T is also a member of the conantokin peptide family and displays biological activity similar to that of con-G, namely, inhibiting ion flow through the NMDAR (*15*), yet con-T is unable to self-associate in the presence of Ca^{2+}(*14*, *22*). To establish the contributions of Gla placement in mediating self-association in the conantokins, we have evaluated the metal ion induced oligomeric tendencies of con-T[K7γ], a peptide that bears homology to con-G with respect to the primary sequence location of Gla residues.

From sedimentation equilibrium analyses, we have demonstrated that the single amino acid substitution of Lys → Gla at sequence position 7 in con-T is sufficient to yield a species that can form a complete, stable dimer in the presence of 20 mM Ca^{2+} (Table 1). Our microcalorimetric data has revealed that con-T[K7γ] has a higher Ca^{2+} binding stoichiometry (ca. 3 mol of Ca^{2+}/mol of monomer or 6 mol of Ca^{2+}/mol of dimer) compared to con-T (ca. 1 mol of Ca^{2+}/mol of peptide). This multiple Ca^{2+} binding was best fit to an equivalent sites model, indicating that no discernible cooperativity is involved in the Ca^{2+}-mediated dimerization of con-T[K7γ]. Furthermore, the covalent trapping of oxidatively folded Cys-containing con-T[K7γ] products, as presented in Figures 5 and 6, highlights the preference for antiparallel strand orientation in the Ca^{2+}-bound dimeric state. These properties of Ca^{2+}-con-T[K7γ] effectively mimic those of con-G (*14*), implying that the mere replacement of Lys^7 with Gla is adequate not only for introducing multiple binding sites for Ca^{2+} but also for inducing the multiple interchain metal ion coordinations that support the dimeric complex. However, the NMDAR inhibitory activity of con-T[K7γ] is 5-fold reduced relative to con-G (*31*), suggesting that the presence of a Gla at sequence position 7 in the con-T context does not permit the recapitulation of con-G-like functional properties. A model for the Ca^{2+}-bridged con-T[K7γ] dimer, similar to that proposed for con-G (*14*), is presented in Figure 8. Residue placement is based on the NMR-derived structures of the apo- and Ca^{2+}-loaded forms of con-T, in which Gla residues 3, 10, and 14 (and presumably Gla^7 of the variant) reside on the same face of the helix, in a nearly linear array (*17*, *21*). This schematic is consistent with both antiparallel strand alignment and a stoichiometry of 6 mol of Ca^{2+}/mol of dimer (assuming that four Ca^{2+} ions bridge the dimer interface and that each strand binds an additional Ca^{2+} at sites outside the core, possibly at Gla^4 (*14*)). In this helical assembly, Gla residues 3, 7, 10, and 14, located at the *a* and *d* helical wheel positions of one

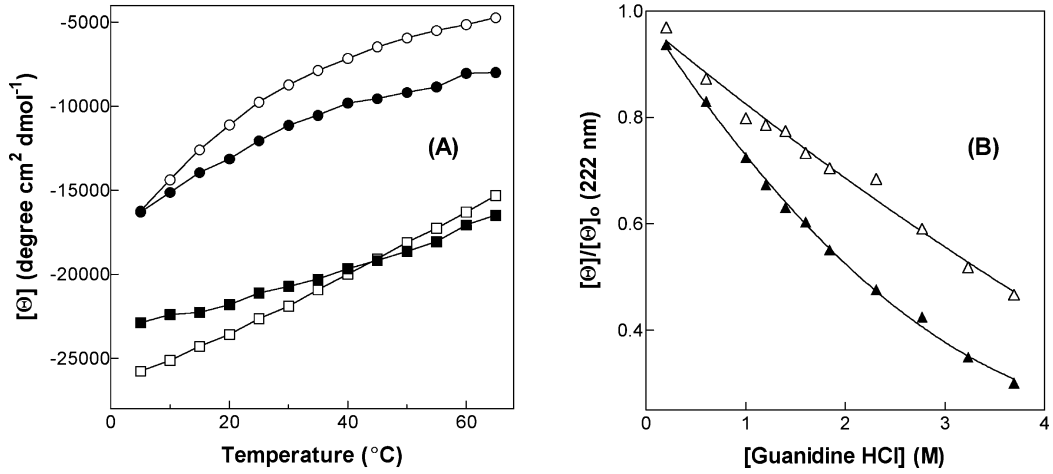

FIGURE 5: CD-monitored thermal and guanidine-HCl denaturations of con-T[K7γ]. (A) Thermal melts of peptide (150 μM in 10 mM $NaBO_3$, 100 mM NaCl, pH 6.5) followed at 208 and 222 nm at low and high Ca^{2+} concentrations: (○) 208 nm, 0.2 mM $CaCl_2$; (●) 222 nm, 0.2 mM $CaCl_2$; (■) 208 nm, 20 mM $CaCl_2$; (□) 222 nm, 20 mM $CaCl_2$. (B) The ratio of molar ellipticities of peptide at 222 nm in the presence [Θ] and absence [Θ_0] of guanidine-HCl were determined at the indicated guanidine-HCl concentrations. Experiments were conducted at 25 °C in 10 mM $NaBO_3$, 100 mM NaCl, 20 mM $CaCl_2$, pH 6.5: (▲) 30 μM con-T[K7γ]; (△) 150 μM con-T[K7γ].

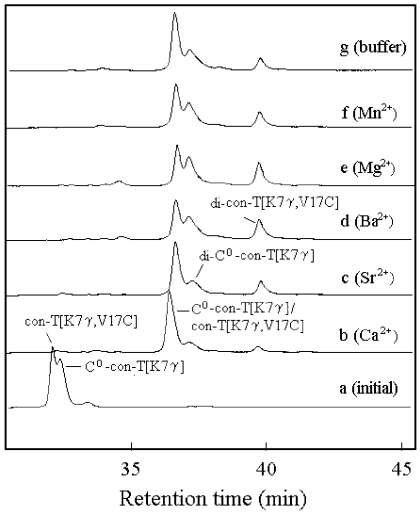

FIGURE 6: HPLC analyses of the equilibrium distribution of oxidation products following mixing of C^0-con-T[K7γ] and con-T[K7γ,V17C] in the presence (b−f) or absence (g) of various metal ions. The folding buffer was 50 mM $NaBO_3$/100 mM NaCl, pH 8.2. The chloride salts of the indicated divalent metal ions were used at a concentration of 20 mM. The initial concentrations of C^0-con-T[K7γ] and con-T[K7γ,V17C] were 360 μM. All chromatograms were obtained as described in Materials and Methods.

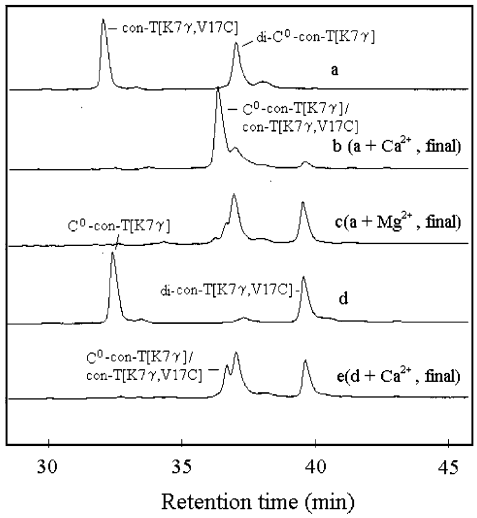

FIGURE 7: HPLC-monitored thiol−disulfide exchange assays of Cys-containing con-T[K7γ] variants. The disulfide-linked homodimeric species, di-C^0-con-T[K7γ] and di-con-T[K7γ,V17C], were separately incubated with con-T[K7γ,V17C] and C^0-con-T[K7γ], respectively. The oxidations were carried out in 50 mM $NaBO_3$/100 mM NaCl, pH 8.2, and either 20 mM $CaCl_2$ or 10 mM $MgCl_2$. Chromatograms represent final equilibrium product distributions.

chain, are bridged (through coordination with a total of four calcium ions) with Gla residues 14′, 10′, 7′, and 3′, respectively, of the complementary chain. Interchain interactions are not supported by Mg^{2+}, Zn^{2+}, nor Mn^{2+} despite the greater binding affinity of these species for the conantokins and their ability to induce high helix content relative to Ca^{2+}. In fact, as shown in Figure 3A, the Ca^{2+}-mediated dimeric complex can be collapsed through addition of Mg^{2+}. This not only implies that the dimerization attending Ca^{2+} binding is incumbent upon proper geometry in the metal−ligand interactions but also suggests that con-T[K7γ] may find utility as a selective and reversible Ca^{2+} sensor.

It should be noted that, as seen with con-G (*14*), Sr^{2+} and Ba^{2+} also promote the oligomerization of con-T[K7γ]. The oxidation product distributions in Figure 7 indicate a pronounced bias for antiparallel strand assembly in the presence of Sr^{2+}, but not in the case of the Ba^{2+}-facilitated oxidation. For the latter ion, this may reflect a tendency to promote oligomerization or aggregation through general carboxylate−Ba^{2+} bridging, as reported for other Gla-containing species (*32*).

In conclusion, the introduction of Gla residue at position 7 in con-T is essential to form a relay of four Gla residues spaced at "*i*, *i* + 4, *i* + 7, *i* + 11" intervals which, in turn, provide a distribution of charges at the helix interface that are optimal for interhelical metal ion coordination. In contrast to con-T, this particular Gla arrangement is deleterious to helical structure in the apo form of the variant, owing to intrahelical charge repulsion (*17*, *18*). Despite identical Gla residue placement in con-T[K7γ] and con-G, the former is more thermally stable and dimerizes to a higher extent than con-G under identical solution conditions. (The fractional dimer content of con-G is 0.48 (*14*), whereas con-T[K7γ] is fully dimeric.) This may be attributable to stabilizing hydrogen bonding contacts between the guanidinium of Arg[13]

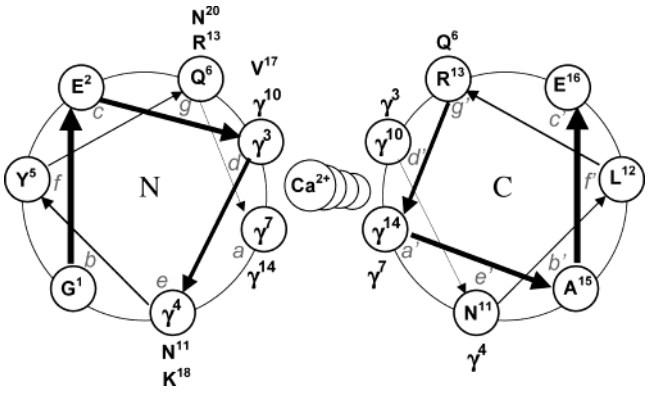

FIGURE 8: Helical wheel representation of the cross-sectional heptad repeats of two con-T[K7γ] strands aligned in antiparallel orientation as mediated by Ca^{2+}. The directions of chain propagation are opposite: For chain 1 (left), the N-terminus is closest to the viewer; for chain 2 (right), the C-terminus is closest to the viewer. Gla^7 and Gla^{14} of chain 1 occupy position *a*, while Gla^3 and Gla^{10} reside at position *d*. These residues pack against the *d*′ and *a*′ residues of chain 2, forming the metal ion chelating core at the dimer interface. Interstrand Gla chelation pairs bridged by four Ca^{2+} ions are γ^3−$\gamma^{14\prime}$, γ^7−$\gamma^{10\prime}$, γ^{10}−$\gamma^{7\prime}$, γ^{14}−$\gamma^{3\prime}$.

and the side-chain carbonyl of Gln^6, as well as the malonate head groups of Gla^4 and the side-chain amide nitrogen of Asn^{11}. The stabilizing nature of similar types of neutral residue−charged residue interhelical interactions has been previously described (*28*). Alternatively, the higher Ca^{2+}-saturated helical content of con-T[K7γ] compared with con-G (67% versus 50%) indicates a greater equilibrium distribution of helix for the former, allowing a greater proportion of folded peptide available for self-association. Overall, our results confirm that Gla-containing helical peptides can be constructed to permit reversible metal ion triggered interchain assembly with a marked preference for antiparallel orientation. The applicability of metal ion sensitive systems of known topology can potentially extend into the de novo design of peptide-based metal-sensoring devices (*33*), tags for purification (*34*), and vehicles for drug delivery (*35*).

REFERENCES

1. Cohen, C., and Parry, D. A. (1994) Alpha-helical coiled coils: more facts and better predictions, *Science 263*, 488−489.
2. DeGrado, W. F., Summa, C. M., Pavone, V., Nastri, F., and Lombardi, A. (1999) *De novo* design and structural characterization of proteins and metalloproteins, *Annu. Rev. Biochem. 68*, 779−819.
3. Oakley, M. G., and Hollenbeck, J. J. (2001) The design of antiparallel coiled coils, *Curr. Opin. Struct. Biol. 11*, 450−457.
4. Kamtekar, S., and Hecht, M. H. (1995) Protein Motifs. 7. The four-helix bundle: what determines a fold? *FASEB J. 9*, 1013−1022.
5. Popot, J.-L., and Engelman, D. M. (2000) Helical membrane protein folding, stability, and evolution, *Annu. Rev. Biochem. 69*, 881−922.
6. Smith, S. P., and Shaw, G. S. (1998) A change-in-hand mechanism for S100 signalling, *Biochem. Cell Biol. 76*, 324−333.
7. Handel, T., and DeGrado, W. F. (1990) *De novo* design of a Zn^{2+}-binding protein, *J. Am. Chem. Soc. 112*, 6710−6711.
8. Regan, L. (1995) Protein design: novel metal-binding sites, *Trends Biochem. Sci. 20*, 280−285.
9. Pessi, A., Bianchi, E., Crameri, A., Venturini, S., Tramontano, A., and Sollazzo, M. (1993) A designed metal-binding protein with a novel fold, *Nature 362*, 367−369.
10. Lieberman, M., and Sasaki, T. (1991) Iron(II) organizes a synthetic peptide into three-helix bundles. *J. Am. Chem. Soc. 113*, 1470−1471.
11. Handel, T. M., Williams, S. A., and DeGrado, W. F. (1993) Metal ion-dependent modulation of the dynamics of a designed protein, *Science 261*, 879−885.
12. Gochin, M., Khorosheva, V., and Case, M. A. (2002) Structural characterization of a paramagnetic metal-ion-assembled three-stranded α-helical coiled coil, *J. Am. Chem. Soc. 124*, 11018−11028.
13. Liu, J., Dai, J., and Lu, M. (2003) Zinc-mediated helix capping in a triple-helical protein, *Biochemistry 42*, 5657−5664.
14. Dai, Q. Y., Prorok, M., and Castellino, F. J. (2004) A new mechanism for metal ion-assisted interchain helix assembly in a naturally occurring peptide mediated by optimally spaced gamma-carboxyglutamic acid residues, *J. Mol. Biol. 336*, 731−744.
15. Haack, J. A., Rivier, J., Parks, T. N., Mena, E. E., Cruz, L. J., and Olivera, B. M. (1990) Conantokin-T. A gamma-carboxyglutamate containing peptide with N-methyl-d-aspartate antagonist activity, *J. Biol. Chem. 265*, 6025−6029.
16. Prorok, M., Warder, S. E., Blandl, T., and Castellino, F. J. (1996) Calcium binding properties of synthetic γ-carboxyglutamic acid-containing marine cone snail "sleeper" peptides, conantokin-G and conantokin-T, *Biochemistry 35*, 16528−16534.
17. Skjærbæk, N., Nielsen, K. J., Lewis, R. J., Alewood, P., and Craik, D. J. (1997) Determination of the solution structures of conantokin-G and conantokin-T by CD and NMR spectroscopy, *J. Biol. Chem. 272*, 2291−2299.
18. Rigby, A. C., Baleja, J. D., Furie, B. C., and Furie, B. (1997) Three-dimensional structure of a γ-carboxyglutamic acid-containing conotoxin, conantokin-G, from the marine snail *Conus geographus*: The metal-free conformer, *Biochemistry 36*, 6906−6914.
19. Rigby, A. C., Baleja, J. D., Li, L., Pedersen, L. G., Furie, B. C., and Furie, B. (1997) Role of γ-carboxyglutamic acid in the calcium-induced structural transition of conantokin G, a conotoxin from the marine snail *Conus geographus*, *Biochemistry 36*, 15677−15684.
20. Chen, Z., Blandl, T., Prorok, M., Warder, S. E., Li, L., Zhu, Y., Pedersen, L. G., Ni, F., and Castellino, F. J. (1998) Conformational changes in conantokin-G induced upon binding of calcium and magnesium as revealed by NMR structural analysis, *J. Biol. Chem. 273*, 16248−16258.
21. Warder, S. E., Prorok, M., Chen, Z., Li, L., Zhu, Y., Pedersen, L. G., Ni, F., and Castellino, F. J. (1998) The roles of individual γ-carboxyglutamate residues in the solution structure and cation-dependent properties of conantokin-T, *J. Biol. Chem. 273*, 7512−7522.
22. Prorok, M., and Castellino, F. J. (1998) Thermodynamics of binding of calcium, magnesium, and zinc to the NMDA receptor ion channel peptidic inhibitors, conantokin-G and conantokin-T, *J. Biol. Chem. 273*, 19573−19578.
23. Holtzer, M. E., and Holtzer, A. (1995) The use of spectral decomposition via the convex constraint algorithm in interpreting the CD-observed unfolding transitions of coiled coils, *Biopolymers 36*, 365−379.
24. Cooper, T. M., and Woody, R. W. (1990) The effect of conformation on the CD of interacting helices: a theoretical study of tropomyosin, *Biopolymers 30*, 657−676.
25. Zhou, N. E., Kay, C. M., and Hodges, R. S. (1993) Disulfide bond contribution to protein stability: positional effects of substitution in the hydrophobic core of the two-stranded alpha-helical coiled-coil. *Biochemistry 32*, 3178−3187.
26. Monera, O. D., Zhou, N. E., Kay, C. M., and Hodges, R. S. (1993) Comparison of antiparallel and parallel two-stranded alpha-helical coiled-coils. Design, synthesis, and characterization. *J. Biol. Chem. 268*, 19218−19227.
27. Monera, O. D., Kay, C. M., and Hodges, R. S. (1994) Electrostatic interactions control the parallel and antiparallel orientation of α-helical chains in two-stranded α-helical coiled-coils, *Biochemistry 33*, 3862−3871.
28. Lumb, K. J., and Kim, P. S. (1995) A buried polar interaction imparts structural uniqueness in a designed heterodimeric coiled coil, *Biochemistry 34*, 8642−8648.
29. McClain, D. L., Woods, H. L., and Oakley, M. G. (2001) Design and characterization of a heterodimeric coiled coil that forms exclusively with an antiparallel relative helix orientation, *J. Am. Chem. Soc. 123*, 3151−3152.
30. Oakley, M. G., and Kim, P. S. (1998) A buried polar interaction can direct the relative orientation of helices in a coiled coil, *Biochemistry 37*, 12603−12610.

31. Blandl, T. (2000) Ph.D. Thesis, University of Notre Dame, Notre Dame, IN,p 68.
32. Stenflo, J., and Ganrot, P. O. (1972) Vitamin K and the biosynthesis of prothrombin. I. Identification and purification of a dicoumarol-induced abnormal prothrombin from bovine plasma, *J. Biol. Chem. 247*, 8160−8166.
33. Chao, H., Bautista, D. L., Litkowski J., Irvin, R. T., and Hodges, R. S. (1998) Use of a heterodimeric coiled-coil system for biosensor application and affinity purification, *J. Chromatogr., B 715*, 307−329.
34. Tripet, B., Yu, L., Bautista, D. L., Wong, W. Y., Irvin, R. T., and Hodges, R. S. (1996) Engineering a *de novo*-designed coiled-coil heterodimerization domain off the rapid detection, purification and characterization of recombinantly expressed peptides and proteins, *Protein Eng. 9*, 1029−1042.
35. Wang, C., Stewart, R. J., and Kopecek, J. (1999) Hybrid hydrogels assembled from synthetic polymers and coiled-coil protein domains, *Nature 397*, 417−420.

BI048796S